STUDY ON THE PERFORMANCE OF RICE STRAW ASH CONCRETE IN LOW-TEMPERATURE ENVIRONMENTS

Fucheng WANG[1*], Heng KANG[2], Pengyue XING[3], Jiabing TIAN[4], Guoliang XIE[5], Xinrong ZHAO[6]

Concrete specimens were made by replacing 0%-20% cement with equal-mass rice straw ash (RSA). They underwent 50, 100, and 150 freeze-thaw (F-T) cycles to test frost resistance, with observations, mass compressive strength analysis, and finite element temperature stress simulation. Results: RSA concrete fills pores via "micro-aggregate effects", reducing F-T pressures and boosting frost resistance. More F-T cycles caused more shedding and lower strength; 5% RSA concrete had max stress at surface edge midpoints.

Keywords: Rice Straw Ash Concrete; Frost Resistance; Mass Loss Rate; Compressive Strength

1. Introduction

During the cement production process, non-renewable energy is utilized [1-2]; leading to carbon emissions and subsequent environmental pollution issues. These challenges have garnered significant attention from experts and scholars alike. To address carbon emissions and promote the healthy and construction industry's sustainable development materials industry, a growing number of scholars are exploring environmentally friendly alternatives to cement [3]. Therefore, the utilization of biomass ash, a by-product of biomass power plants, serving as an admixture for the partial replacement of cement in concrete has developed into a key research area. This topic has garnered considerable attention

[1]* College of Engineering, Heilongjiang Bayi Agricultural University, Daqing 163319, corresponding author, Chinafuchengwang@byau.edu.cn
[2] College of Civil Engineering and Water Conservancy, Heilongjiang Bayi Agricultural University, Daqing 163319, China
[3] College of Civil Engineering and Water Conservancy, Heilongjiang Bayi Agricultural University, Daqing 163319, China
[4] College of Civil Engineering and Water Conservancy, Heilongjiang Bayi Agricultural University, Daqing 163319, China
[5] College of Civil Engineering and Water Conservancy, Heilongjiang Bayi Agricultural University, Daqing 163319, China
[6] College of Energy and Building Engineering, Shandong Huayu University of Technology, Dezhou 253034, China

from scholars who are conducting in-depth studies on its implications and applications.

In recent times, many scholars have explored the properties of specific kinds of biomass ash. Studies have revealed that rice husk ash contains up to 91.2% silica (SiO_2) [4], while the combined concentrations of SiO_2 and alumina (Al_2O_3) in corn straw ash exceed 70% [5]. Furthermore, wheat straw ash has been reported to possess an active substance content of 80.16% [6]. The experimental evidence demonstrates that biomass-derived ash exhibits potential as a sustainable cementitious substitute in civil engineering applications. Bheel et al. demonstrated that partial cement substitution with wheat straw ash improves concrete's mechanical properties—specifically compressive strength, tensile strength, and flexural strength—were analyzed [7]. Romano J S et al conducted compressive strength tests on concrete made from rice husk ash with different substitution rates and proposed that the substitution rate of 10% results in the best compressive strength effect [8-9]; Ramasamy V found that at a substitution rate of 20% for rice husk ash, the sulfate corrosion resistance of concrete improved by 11.20% [9]. When biomass ash partially replaces cement in concrete, it not only decreases permeability [10], but also enhances its thermal insulation properties and improves the corrosion resistance of reinforcing steel [11-12]. However, this type of substitution may lower the bond strength of concrete and reinforcing steel [13]. Hence, partially replacing cement with biomass ash at dosages controlled to ensure performance demonstrates technical viability.

Rice is one of the principal crops cultivated in China. The sown area reached 29,450.1 thousand hectares in 2022 and decreased to 28,949.1 thousand hectares in 2023, respectively [14-15]. The production of rice straw increased from 202,883,000 tons in 2011 to 208,495,000 tons in 2022, reflecting an annual average growth rate of 0.25%[16]. The efficient use of RSA cannot merely enable the reuse of agricultural resources but also raise the earnings of farmers [17]. Nevertheless, currently, researchers primarily concentrate on the mechanical characteristics of RSA concrete, while there are relatively fewer studies on its frost resistance. Hence, carrying out research on the freezing resistance of RSA concrete is of certain significance for its popularization and application.

This paper aims to investigate and elucidate the mechanisms underlying the frost resistance of RSA concrete. Quick F-T cycle tests were carried out on RSA concrete specimens having different substitution rates, undergoing 50, 100, and 150 cycles. The observable phenomena exhibited by the specimens following these F-T cycles were analyzed to explore the patterns in mass loss ratio and variations in compressive strength. The temperature stress simulation of RSA concrete specimens with a substitution rate of 5% was performed using finite element software, resulting in the identification of the temperature stress distribution characteristics of RSA concrete. This research offers valuable insights into the

resource utilization of rice straw and contributes to the preparation and practical engineering applications of RSA concrete.

2. Research Materials and Approaches

2.1 Experimental material

The cement (C) employed was the P·O 42.5 ordinary Portland cement manufactured by Daqing Oilfield Cement Co., Ltd., with the brand name of Youlong.

The fine aggregate utilized in this study was river sand (S) procured from the construction materials market in Daqing City. In accordance with the "Standard for Construction Sand (GB/T 10684-2022)", various parameters of the sand were tested. The fineness modulus was determined to be 2.68, and the apparent density was measured at 2.565 g/cm³.

The rice straw ash (RSA) was produced through the natural outdoor combustion of rice straw sourced from the experimental field of Heilongjiang Bayi Agricultural University. Following processes such as grinding and sieving, the particle size of the ash was adjusted to meet the specifications required for cementitious materials. After treatment, the RSA exhibited a black coloration, with SiO_2 content reaching 76.88%. Detailed information on the chemical constituents of cement and RSA is provided in Table 1.

Table 1

Chemical constituents of cement and RSA

Chemicalconstituents（%）	SiO_2	K_2O	Na_2O	CaO	MgO	SO_3	P_2O_5	Fe_2O_3	Al_2O_3	Other
C	21.08			64.59	1.29	1.89		5.68	5.47	
RSA	76.88	11.05	0.85	4.37	1.69	2.69	1.66	0.35	0.27	0.19

The natural coarse aggregate (NCA) utilized in this study was ordinary crushed stone, sourced from the construction materials market in Daqing City. This material exhibits an apparent density of 2.70 g/cm³ and has a maximum particle size of 20 mm.

The high-efficiency superplasticizer is a polycarboxylate-based high-performance additive developed by Tianjin Weihe Technology Development Co., Ltd.

The water(W) used for stirring is obtained from the municipal water supply of Daqing City. The appearance characteristics of some of the materials utilized are illustrated in Fig. 1.

2.2 Experimental methods

Within this research, RSA was utilized to replace cement at mass ratios of 0%, 5%, 10%, 15%, and 20%. RSA-incorporated concrete specimens (with

dimensions 100 *mm* × 100 *mm* × 400 *mm*) were prepared following GB/T50082-2024 specifications (Chinese National Standard for concrete durability testing). The mass mix proportion is specified in Table 2. Following the pouring of the specimens, they were allowed to cure for a period of 48 hours before demolding; subsequently, the specimens were assigned identification numbers. Due to the relatively slow reaction kinetics of RSA particles [18] it was necessary to place the specimens in a standard curing box for a duration of 56 days to fully utilize the potential benefits of RSA.

Fig.1 Raw material sample picture

Table 2

Mix ratio of frost resistance of RSA

Number	Substitution rate（%）	C (kg/m^3)	RSA (kg/m^3)	W (kg/m^3)	S (kg/m^3)	NCA (kg/m^3)	WRA (kg/m^3)	W/B
B0	0	350	0	140	642.6	1247.4	3.5	0.4
B5	5	332.5	17.5	140	642.6	1247.4	3.5	0.4
B10	10	315	35	140	642.6	1247.4	3.5	0.4
B15	15	297.5	52.5	140	642.6	1247.4	3.5	0.4
B20	20	280	70	140	642.6	1247.4	3.5	0.4

Note: B0, B5, B10, B15, and B20 respectively denote the specimens with RSA replacement rates of 0%, 5%, 10%, 15%, and 20%.S is the abbreviation for sand, and W/B stands for the water-binder ratio.

After the curing period, rapid freeze-thaw (F-T) cycle tests were conducted using an HC-HDK9/Y F-T testing machine with a temperature range of -20℃ to 20℃. Each cycle lasted 2 hours, with the total number of cycles set at 50, 100, and 150. Before the test and after every 50 cycles, the specimens were dried, weighed, and the mass loss rate was calculated using the weighing method. Finally, the concrete compressive strength was measured using a WAW-1000 Universal Testing Machine (UTM).

2.3 Finite element simulation

Utilizing a sequential coupled thermal stress analysis approach, numerical simulations were conducted to investigate the F-T cycles of RSA concrete (with a substitution rate of 5%), which demonstrated the highest frost resistance in the experimental evaluations. According to the principles of thermodynamics [19], the matrix representation utilized in thermal analysis is expressed as Equation (1):

$$[C]\{T_1\}+[\lambda]\{T\}=\{Q\} \tag{1}$$

Wherein: $[C]$is the specific heat capacity matrix; $\{T_1\}$ is the first-order deriv ative of T with respect to time. $[\lambda]$is the heat transfer matrix. $[T]$is the vector of nod e temperatures. $\{Q\}$ is the heat flux rate vector for the node.

The formulation of the transient heat conduction boundary is articulated in Equation (2):

$$-\lambda\frac{\partial T}{\partial n}=\beta\left(T-T_\alpha\right) \tag{2}$$

In the equation: β is the surface heat transfer coefficient between the model and the surrounding environment on the boundary; T_α is the temperature of the surrounding fluid.

A model of the RSA concrete material component, measuring $100\,mm \times 100\,mm \times 400\,mm$, was developed. The mesh element type utilized for this model was heat transfer, and the material properties are detailed in

Table 3

Thermodynamic Parameters Table. The analysis step is categorized as heat transfer, with the response type being transient. The F-T cycle effect is implemented by setting an amplitude, with a temperature range of -20 to 20°C. One complete cycle lasts for 2 hours. To enhance the accuracy of the computational results, a smaller analysis time step is preferred; thus, the time step has been set to 0.1 hours. The number of F-T cycles considered are 50, 100, and 150 times, corresponding to output durations of 100 hours, 200 hours, and 300 hours respectively. The model's temperature boundary condition is established at 5°C.

Table 3

Thermodynamic Parameters Table

Density (kg/m^3)	Specific heat [J/(kg·K)]	Conductivity [W/(m·K)]	Expansion (1/℃)	Data source
2400	1000	1.74	1e^{-5}	Document[26]

The model utilized in the temperature field is replicated for static analysis. When analyzing the thermal stress field, the mesh partitioning is kept consistent with that used for the temperature field; In the analysis of the thermal stress field,

the mesh division is consistent with that of the temperature field at 10 mm, as the mesh division has minimal impact on the results [20] Additionally, the analysis step type is adjusted to static and general. Subsequently, the calculation results obtained from simulating the temperature field are incorporated into the model as a predefined field to effectively simulate frost heave.

3. Analysis of experimental results

3.1 Superficial phenomena

The observable morphology serves as an intuitive representation of concrete that has been subjected to F-T cycles. To a certain extent, it can also reflect the degree of damage sustained by the concrete [21]. The apparent morphologies of RSA concrete specimens with varying substitution rates once they had undergone 0, 50, 100, and 150 F-T cycles are illustrated in Fig. 4,5,6 and 7, respectively.

（a）0% of RSA　(b) 5% of RSA　（c）10% of RSA　（d）15% of RSA　（e）20% of RSA

Fig. 2 Appearance after 0 cycles of F-T

（a）0% of RSA　(b)5% of RSA　（c）10% of RSA　（d）15% of RSA　（e）20% of RSA

Fig. 3 Appearance after 50 cycles of F-T

（a）0% of RSA　(b)5% of RSA　（c）10% of RSA　（d）15% of RSA　（e）20% of RSA

Fig. 4 Appearance after 100 cycles of F-T

（a）0% of RSA　(b) 5% of RSA　（c）10% of RSA　（d）15% of RSA　（e）20% of RSA

Fig. 5 Appearance after 150 cycles of F-T

With the growing number of F-T cycles, there is a concomitant increase in the number of surface pores on the specimens, and the corners gradually become more rounded. It can be seen from Fig. 4 that the surface of the specimen, which had not been subjected to F-T cycles, was sleek and level. Conversely, as shown in Fig. 5 and 6, after experiencing 50 and 100 F-T cycles respectively, the surface of the specimen demonstrated notable roughness, along with the detachment of fine sand. Notably, the most severe damage occurred at both the central area of the specimen's surface and along its peripheral edges. When the replacement rate of RSA is set at 5% or 10%, the extent of surface damage observed after 50 or 100 F-T cycles is less pronounced compared to that of conventional concrete. It can be observed from Fig. 7 that after undergoing 150 F-T cycles, all specimens demonstrate a phenomenon in which the cement mortar detaches in block-like fragments, thereby revealing the coarse aggregates with relatively large particle sizes.

3.2 Mass loss rate

Mass loss serves as one of the evaluation indices for the deterioration degree of concrete [22]. As depicted in Fig. 8, the mass loss rates for both ordinary concrete and RSA concrete exhibit a positive correlative relation to the count of F-T cycles experienced. As can be observed in Fig. 9, for both ordinary concrete and RSA concrete specimens, the mass loss rate exhibits a trend of initially decreasing followed by an increase as the RSA substitution rate rises, across 50, 100, and 150 F-T cycles. Specifically, after undergoing 50 F-T cycles, the minimum mass loss rate recorded is 0.60% at an RSA substitution rate of 10%. In contrast, for the conditions of 100 and 150 F-T cycles, the minimum mass loss rates are found to be 1.03% and 14.67%, respectively, when the RSA substitution rate is set at 5%. The rationale behind this phenomenon is rooted in the fact that when the replacement rate of RSA is between 5% and 10%, the active SiO_2 present during the hydration process engages in a pozzolanic reaction with calcium hydroxide, which is generated by the hydration of cement. This interaction results in the generation of a large quantity of calcium silicate hydrate (C-S-H) gel. Consequently, there is a reduction in the internal porosity of the concrete, leading to increased compactness. As a result, during F-T cycles, RSA concrete experiences lower hydrostatic and

osmotic pressures compared to ordinary concrete. This translates into reduced damage levels and a smaller mass loss rate relative to other groups.

When subjected to 50 F-T cycles, the mass loss rate of ordinary concrete was observed to be 0.81%. In contrast, when the replacement rates of RSA were set at 5% and 10%, the corresponding mass loss rates were recorded at 0.77% and 0.60%, respectively. These values represent reductions of 0.04% and 0.21% compared to that of ordinary concrete. After 100 F-T cycles were performed, the mass loss rates of RSA concrete with replacement rates of 5% and 10% were observed to be 1.03% and 1.18% respectively, values that are lower than the 1.45% of ordinary concrete. In contrast, the mass loss rates increased to 3.24% and 1.62% when the replacement rates were set at 15% and 20%, respectively, indicating a higher deterioration compared to ordinary concrete. High RSA content increases porosity and pore connectivity, allowing easier water ingress. Subsequent freezing exerts excessive pressure, causing surface cracking and mass loss.As illustrated in Fig. 8, upon reaching 150 F-T cycles, the mass loss rate of each specimen exhibited a significant increase. The mass loss rate of ordinary concrete was documented at 35%, whereas the RSA concrete with a substitution rate of 5% demonstrated a mass loss rate of 14.67%. This represents an increase of 13.64% compared to the results observed after 100 F-T cycles. It can be inferred that RSA concrete with a substitution rate of 5% exhibits superior frost resistance compared to ordinary concrete when subjected to F-T cycles of fewer than 100 times. However, after 150 F-T cycles, both ordinary and RSA concrete experience significant damage.

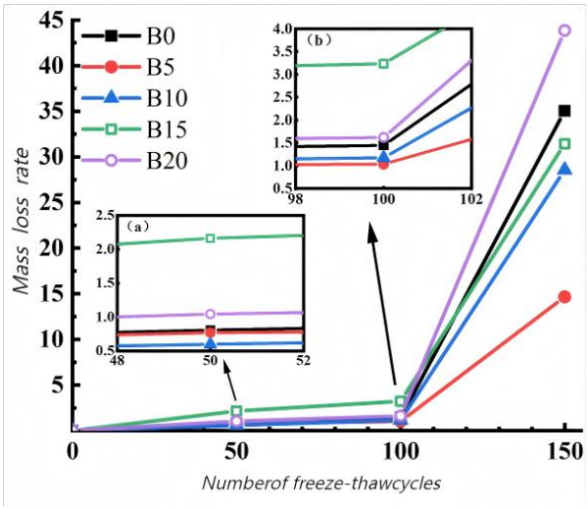

Fig. 6 Mass loss rate vs. number of F-T cycles

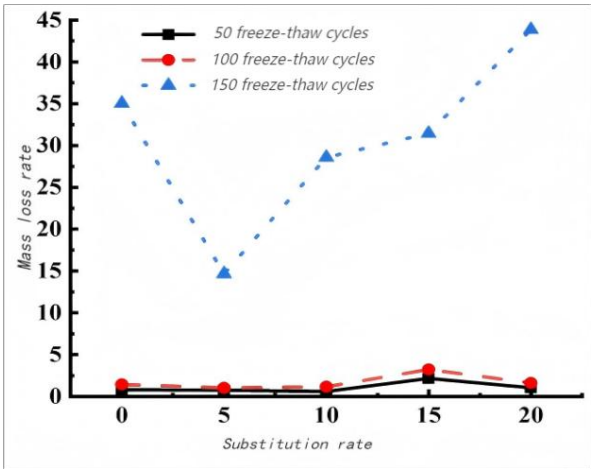

Fig. 7 Mass loss rate and substitution rate

3.3 Compressive strength

The variation of the specimens' compressive strength with the number of F-T cycles is shown in Fig. 10. As shown in Fig. 10, the compressive strengths of ordinary concrete and RSA concrete both show a tendency to decrease gradually as the number of F-T cycles increases. After 50 F-T cycles, the compressive strength of RSA concrete with a 10% replacement rate was measured at 24.9 MPa, surpassing that of ordinary concrete (23.2 MPa) by 7.3%. However, following 100 cycles, it was found that the compressive strength of RSA concrete was lower than that of plain concrete. By 150 cycles, both types of concrete approached nearly 100% strength loss.

RSA, characterized by fine particles, enhances the particle gradation of cement when used as a replacement, thereby reducing porosity and increasing concrete density. When the replacement rate is below 10%, the reactive SiO_2 in RSA reacts with cement hydration products to form new gel-like substances, further decreasing pore volume. This refinement of the pore structure limits water ingress into the concrete matrix, reducing hydrostatic and osmotic pressures during F-T cycles, which mitigate structural damage and improves compressive strength. In contrast, at replacement rates exceeding 15%, the dilution effect becomes dominant. As RSA replaces a significant portion of the Portland cement clinker, the absolute amount of primary hydration products generated by cement hydrolysis decreases, leading to a less dense matrix. Although the pozzolanic reaction between RSA and CH continues, the rate is relatively slow. Consequently, the excess RSA particles act primarily as inert fillers rather than active binders at this stage. This combination between reduced hydration product density and the physical presence of unreacted particles creates a more porous microstructure with weaker interfacial bonds, resulting in the observed reduction in compressive strength.

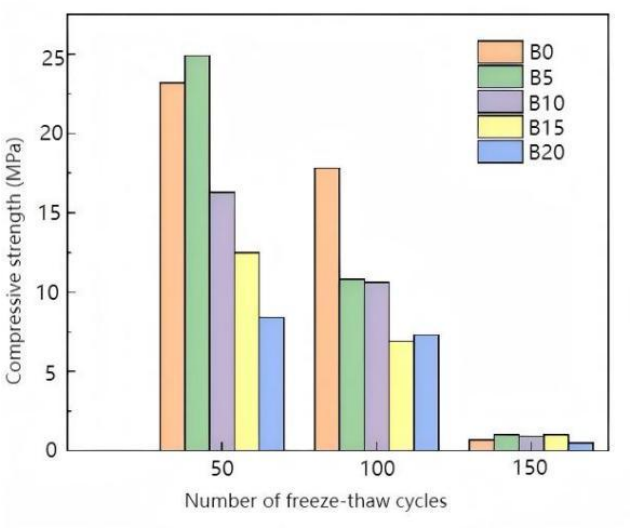

Fig. 8 Compressive strength and F-T cycles

3.4 Analysis of thermal stress simulation results

Thermal stress refers to the internal stress generated in an object when it is unable to freely expand or contract due to fluctuations in temperature, or when there are variations in temperature among different regions within the object. The transfer of heat within concrete is a time-dependent process. Following a certain duration of heat transfer, a temperature gradient develops between the internal and external parts of the concrete specimen, consequently leading to the generation of thermal stress. Throughout the F-T cycles that the specimen undergoes, variations in temperature across different parts result in thermal stress, which ultimately contributes to crack formation within the concrete specimen. Furthermore, continuous, repetitive freeze-thaw cycling markedly promotes both the initiation and the propagation of such cracks.

The temperature stress cloud diagrams (Mises equivalent stress) of RSA concrete specimens after 50, 100, and 150 F-T cycles are presented in Figs. 11, 12, and 13, respectively. The maximum Mises equivalent temperature stress values after these cycles are summarized in Table 4. It can be observed that the temperature stress values of the specimens exhibit a gradual increase with the number of F-T cycles. When subjected to 50 F-T cycles, the minimum temperature stress generated is measured at 2.995×10^{-6}MPa. In contrast, after undergoing 100 and 150 F-T cycles, the maximum temperature stress values are approximately recorded as 3.236 MPa and 3.244 MPa, respectively. As illustrated in Fig. 11, 12, and 13, during the F-T cycling process, the maximum thermal stress occurs at both the center of the specimen's surface and at the midpoint of its edges. This stress gradually diminishes from these central locations towards each of the four sides. Consequently, during

the F-T cycling process, both the center of the specimen surface and the midpoint of its edge are most significantly affected by F-T cycles, resulting in the most severe damage. This observation aligns with the damage phenomena noted at the specimen's edge following F-T treatment as discussed in Section 2.3.1 of this paper.

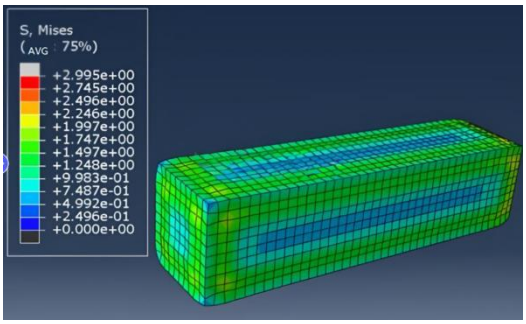

Fig. 9 Temperature stress after 50 F-T cycles

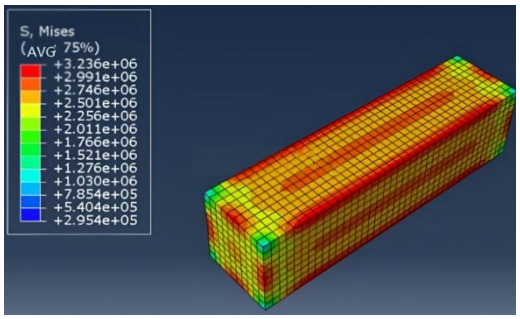

Fig. 10 Temperature stress after 100 F-T cycles

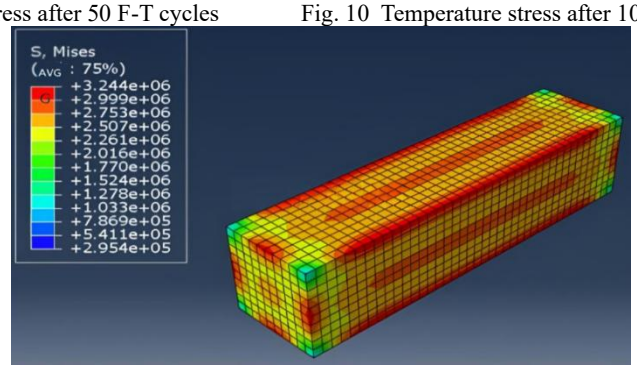

Fig. 11 Temperature stress after 150 F-T cycles

Table 4

Maximum Mises Equivalent Temperature Stress of RSA Concrete Specimens After F-T Cycles

F-T cycles	RSA concrete
50	2.995×10^{-6}Mpa
100	3.236 Mpa
150	3.244 Mpa

Note: Values correspond to RSA concrete with a substitution degree of 5%

3.5 The mechanism of frost resistance in RSA concrete

Classical theories on concrete F-T damage mainly include hydrostatic and osmotic pressure theories. The former holds that pore water freezes and expands during F-T cycles, driving unfrozen water outward to generate hydrostatic pressure [23]; damage occurs when this pressure exceeds concrete’s tensile strength. The latter suggests pore liquid contains soluble salts: macropore water freezes first as

temperature drops, increasing solution concentration, while micropore water remains unfrozen with stable concentration. This gradient triggers liquid migration from micropores to macropores, forming osmotic pressure[24] that induces cracking. Both theories attribute F-T damage to temperature-induced changes in pore liquid volume or concentration, which enhance internal forces and cause concrete failure. Notably, small air pores from air-entraining agents are key to improving F-T resistance, requiring further discussion. These pores act as pressure relief valves: frozen water expansion pressure is dissipated by air compression, avoiding excess tensile stress and cracking. They also interrupt capillary channels, slowing unfrozen water migration and reducing osmotic pressure buildup. Proper air content and uniform distribution significantly boost F-T durability. Clarifying the superplasticizer's air-entraining effect is essential. Traditional superplasticizers lack obvious air-entraining properties, and some even release air. Modified polycarboxylate-based types may have weak air-entraining capacity, but with unstable, hard-to-control air volume versus dedicated agents. If non-air-entraining, concrete air content depends on cement, aggregate, or added air-entraining agents. A weak effect requires evaluating bubble volume, size, and distribution to avoid misjudging dedicated agents' role—critical for accurate F-T resistance analysis and engineering references.

The frost resistance improvement in RSA concrete arises from two dominant mechanisms.Firstly, there is the "filler effect." By substituting cement with RSA of equivalent mass but smaller particle size during the concrete mixing process, it is possible to optimize the particle size distribution and improve the pore structure. This substitution reduces the internal porosity of the concrete and increases its density, thereby contributing to an improvement in frost resistance to a certain extent. Another contributing factor is the "pozzolana reaction." Reactive SiO_2 constitutes a significant portion of RSA. Active SiO_2 undergoes secondary hydration with cement-derived calcium hydroxide, producing abundant C-S-H gel through pozzolanic reactivity [25], as illustrated in Fig. 14. Meanwhile, RSA exhibits a porous structure. Following thorough blending in the initial stage, RSA is uniformly distributed within the cement paste. At the early stages of the cementitious material's hydration, RSA absorbs and retains some free water, subsequently releasing it throughout the hydration process, thereby exerting an "internal curing effect." [26] This phenomenon facilitates the generation of additional C-S-H gel during cement hydration, which contributes to a reduction in internal porosity within concrete and enhances its frost resistance. Thus, RSA concrete's internal structure has a higher density relative to ordinary concrete. RSA concrete contains a reduced amount of free water, leading to lower hydrostatic and osmotic pressures during the F-T cycles. Consequently, compared to conventional concrete, RSA concrete has better frost resistance.

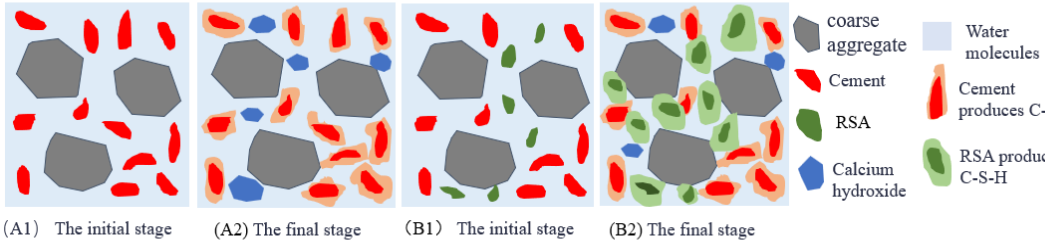

Fig. 12 Changes in pore structure after replacing cement with RSA. (A): Portland cement concrete; (B): 5% RSA replacement rate.

4. Discussion

RSA enhances the F-T resistance of concrete by leveraging two mechanisms: the "micro-aggregate effect" and the "active effect." A comparative analysis was conducted on the apparent phenomena, mass loss rate, and compressive strength between RSA concrete and ordinary concrete. The results indicated that RSA concrete with a substitution rate of 5% demonstrated optimal frost resistance. A numerical simulation of thermal stress was performed on RSA concrete with a substitution rate of 5%. The results demonstrated that the thermal stress increased progressively along with the F-T cycle count. The maximum thermal stress took place not only at the center of the surface that belongs to the specimen but also along the midpoints of its edges. This observation aligns with the evident damage patterns observed in RSA concrete following F-T cycles, indicating that during frost heaving damage, it is primarily the center of the surface and the midpoints of the edges that experience initial failure.

5. Conclusion

(1) The enhanced frost resistance of RSA concrete can be attributed to two primary factors. To start with, the "filler effect" arises from the smaller particle size of RSA relative to cement particles, which in turn optimizes particle gradation and aids in concrete densification. Second, there is the "active effect," wherein active SiO_2 interacts with the hydration products of cement, resulting in the formation of new C-S-H-type cementitious compounds that fill pores and further enhance the density of the concrete. The reduction of detrimental pores results in a marked reduction in both hydrostatic and osmotic pressures in RSA concrete during F-T cycles, thereby enhancing its frost resistance.

(2) Throughout F-T cycles, both RSA concrete and ordinary concrete show a rising trend in mass loss rate and a declining trend in compressive strength as the cycle count increases. RSA concrete with a 5% replacement rate shows a lower mass loss rate compared to ordinary concrete when the F-T cycle count is under

100. Moreover, its compressive strength is higher than ordinary concrete's when the F-T cycle count is below 50. Therefore, under F-T conditions, the optimal replacement rate for RSA in concrete applications is determined to be 5%.

(3) The temperature stress model for RSA concrete subjected to F-T cycling with a 5% substitution rate was developed. The simulation outcomes indicated that the thermal stress rose steadily as the F-T cycle count increased. Upon reaching 150 cycles, the maximum temperature stress recorded at the midpoint of the specimen's edge was found to be 3.244 MPa. During F-T cycling, the peak thermal stress is detected at both the center of the surface of the specimen and along the mid - points of its edges. This stress gradually diminishes from these central locations towards the periphery. Such observations align with the evident damage phenomena exhibited by RSA concrete following F-T cycles.

The disposal of RSA through methods such as burial poses a significant risk of environmental pollution. Residual heavy metals, additives, and pathogens in RSA can leach into soil and groundwater via rainfall, impairing soil quality, contaminating water supplies, and threatening ecosystems. Meanwhile, anaerobic decomposition of organic matter in buried RSA releases methane, and large-scale burial consumes arable land. The effective utilization of RSA not only plays a crucial role in environmental protection but also generates economic benefits for farmers. As a concrete admixture, RSA can reduce the consumption of cement and energy, thereby contributing to the sustainable development of society.

Acknowledgments

This thesis has been funded by the Doctoral Research Foundation Project (XDB202205); We would like to express our gratitude for the funding of the school level Three Vertical and Three Horizontal Project (ZRCPY202202) and the 2025 school enterprise cooperation project (Industrial Application Research of Rice Straw Ash) of Jian Sanjiang Branch.

R E F E R E N C E S

[1]. *Balbi E P, Comodi P, Cambi C, et al*. Wood biomass ash, municipal solid waste ash, and recycled concrete from construction demolition waste as supplementary cementitious materials in fine graded granular mixtures[J]. Construction and Building Materials, 2025, 498: 144016.

[2]. *Jiao H C, Li Y F, Yuan J*. Research progress on use of carbon nanotubes in cementitious grouting materials[J]. Journal of Sustainable Cement-Based Materials, 2024, **13**(7): 1090-1106.

[3]. *Sharma U, Gupta N, Bahrami A*, et al. Behavior of fibers in geopolymer concrete: A comprehensive review[J]. Buildings, 2024, **14**(1): 136.

[4]. *Zheng S S, LI HC R S*. Experimental study on chloride ion penetration resistance and frost resistance of rice husk ash and cellulose fiber admixed concrete[J]. Journal of Hunan University (Natural Sciences), 2024, **51**(5): 193-206.
[5]. *Wei Y, Yin Y, Tahir M H*, et al. Effects of washing treatments and ashing conditions on SiO2 crystalline transitions in rice husk ash[J]. Biofuels, Bioproducts and Biorefining, 2025, 19(3): 746-758.
[6]. *Šupić S, Malešev M, Radonjanin V*, et al. Reactivity and pozzolanic properties of biomass ashes generated by wheat and soybean straw combustion[J]. Materials, 2021, **14**(4): 1004.
[7]. *Katman H Y B, Khai W J, Bheel N*, et al. Workability, strength, modulus of elasticity, and permeability feature of wheat straw ash-incorporated hydraulic cement concrete[J]. Buildings, 2022, **12**(9): 1363.
[8]. *Muñoz-Castillo A, Sánchez-Soto P J, Eliche-Quesada D*. Valorisation of rice husk ash as an activator in the preparation of alkali-activated cements based on electric arc furnace slag[J]. Archives of Civil and Mechanical Engineering, 2025, **25**(3): 155.
[9]. *Duong N T, Van Duc B, Van Phi D*. Effect of Rice Husk Ash Incorporation on the Strength Development and Microstructural Properties of Stabilized Clayey Soil[J]. Arabian Journal for Science and Engineering, 2025: 1-11.
[10]. *Olii M R, Ali A Z P M, Djau R A*, et al. Enhancing Compressive Strength of Self-Compacting Concrete (SCC) through Rice Husk Ash and Superplasticizer Incorporation[J]. Jurnal Teknik, 2025, **23**(1): 229-241.
[11]. *Nassar R U D, Room S*. Strength, Durability, and Microstructural Characteristics of Binary Concrete Mixes Developed with Ultrafine Rice Husk Ash as Partial Substitution of Binder[J]. Civil Engineering and Architecture, 2025, **13**(1): 595-611.
[12]. *Cui Lijun, Qiao Hongxia, Cao Feng*, et al. Damage Characteristics of Highland Barley Straw Ash Modified Magnesium Oxychloride Cement Mortar for Protecting Reinforced Concrete[J]. Bulletin of the Chinese Ceramic Society, 2024, **43**(9): 3282-3293.
[13]. *Sathe S, Devsale A*. Influence of corrosion on bond strength in reinforced recycled aggregate concrete with fly ash[J]. European Journal of Environmental and Civil Engineering, 2025: 1-34.
[14]. National Bureau of Statistics, 2022. Announcement by the National Bureau of Statistics on the 2022 Grain Production.
[15]. National Bureau of Statistics, 2023. Announcement by the National Bureau of Statistics on the Early Rice Crop Production for 2023.
[16]. *Liu J, Yan X, Meiyi Z*, et al. Analysis of yield distribution and utilization of crop straw resources in China[J]. Journal of Agriculture Resources and Environment, 2025, **42**(3): 751.
[17]. *Pandey D, Pandey R, Mishra R K*. Evaluation Of Geopolymer Concrete Towards Sustainable Construction Material[J]. Technische Sicherheit, 2024, **24**(4): 329-338.
[18]. *Wang,fucheng*., 2022. Investigation on Preparation Mechanism and Application of Rice Straw[D]. Heilongjiang Bayi Agricultural University.
[19]. *Zhang J, Chen Y, Du R*, et al. Experimental study and numerical simulation verification of the macro-and micromechanical properties of the sandstone–concrete interface under freeze–thaw cycles[J]. Construction and Building Materials, 2024, 432: 136584.
[20]. *Chen, Y., Wu, S. H., & Ding, J. W*. (2023). Review on the influence of physicochemical properties of rice husk ash on main properties of cement-based materials. Concrete, (7), 97-103.
[21]. *Chen, X. L*. (2023). Numerical simulation and analysis of reinforced concrete structures under sulfate attack conditions based on ABAQUS [D]. Ningxia University.
[22]. *Gan L, Liu Y, Shen Z*, et al. Damage evolution law of concrete under sulfate attack and freeze-thaw cycle[J]. J. Huazhong Univ. Sci. Technol. (Nat. Sci. Ed.), 2023, **51**(11): 134-141.

[23]. *Hu Y, Liu R, Su Y*, et al. Rice husk ash ultra-high-performance concrete: mechanical properties and microstructure analysis after freeze-thaw cycles[J]. Journal of Sustainable Cement-Based Materials, 2025: 1-14.
[24]. *Ma Q, Duan Z, Wang J*, et al. Frost resistance and improvement techniques of recycled concrete: a comprehensive review[J]. Frontiers in Materials, 2024, 11: 1493191.
[25]. *Huang D, Wang X, Feng Y*, et al. The mechanical properties and microstructure of early frozen concrete[J]. Construction and Building Materials, 2025, 493: 143127.
[26]. *Zhao,Xinrong*., 2024. Research on Frost Resistance of Rice Straw Ash Concrete[D]. Heilongjiang Bayi Agricultural University.